Anisotropic etching of silicon crystals in KOH solution

Part I *Experimental etched shapes and determination of the dissolution slowness surface*

C. R. TELLIER, A. BRAHIM-BOUNAB
Laboratoire de Chronométrie Electronique et Piézoélectricité, Ecole Nationale Supérieure de Mécanique et des Microtechniques, La Bouloie, Route de Gray, 25030 Besancon Cedex, France

The anisotropic etching behaviour of various crystalline silicon plates in an aqueous KOH solution was studied. Variations of the etch rate with the angle of cut related to singly-rotated plates have been determined and orientation effects in the out-of-roundness profiles related to various $\{hk0\}$ sections have been analysed in terms of crystal symmetry. In addition, changes in the surface texture with crystal orientation were systematically investigated. All the experimental results furnished evidence for a dissolution process governed by the crystal orientation. A procedure has been proposed to derive the dissolution slowness surface from experiments starting from a tensorial representation of the anisotropic etching.

1. Introduction

During the last four decades, the anisotropic etching of crystal has been used to obtain a measure of crystal perfection [1-9]; in particular, interest has been concentrated on the etch-pit method which appears to be a simple process by which to detect dislocations on semiconductor surfaces [1-3, 8] or quartz surfaces [4, 5, 7]. But in the past few years, several attempts [10-25] have been made to apply the photolithographic process to the micromachining of mechanical devices which constitute the sensing element of silicon-integrated sensors or of silicon-based microresonators. The fabrication technique always involves an anisotropic wet-etching process and works related to silicon wafers are generally limited to $\{100\}$ and $\{110\}$ surfaces [10-12, 14, 16, 23-29]. When using anisotropic etching, the main difficulty in micromachining arises from the lateral underetching and from the corner undercutting [23-29]. Recently, some methods involving mask-compensation techniques [26, 28, 29] have been proposed to reduce corner undercutting.

Moreover, the performance of a micromachined sensor is essentially determined by the final geometrical feature of the sensing element, including the topology of etched surfaces for structures such as diaphragms. The optimization of the sensor geometry passes through the theoretical prediction of etched shapes as soon as the fabrication process starts with differently oriented wafers, in order to enhance the sensitivity and the resolution of the sensors [30, 31].

Over the last few years, the prediction of etching shapes has often been based on the kinematic model proposed by Franck [33, 34] which provides the necessary tools [34-36] to construct geometrically the etching shapes encountered in localized etching at an inert mask. Tellier and co-workers have recently shown that it is possible to predict the exact geometry of etched micromechanical devices using a tensorial analysis [37-43] of the anisotropic process. This may be done as soon as the representative surface of the dissolution slowness vector, *L*, [43-45] can be extracted from etch data with sufficient accuracy. The paper will be divided into three parts. In part I, experimental results related to etched shapes are intensively investigated. Changes in the geometrical features of differently oriented silicon surfaces, as well as in the limiting shapes of various starting cylindrical crystals induced by etching in KOH solutions, are reported and analysed. Then a procedure is proposed to derive the dissolution slowness surface of silicon crystal. In the second part, graphical simulations of etched two-dimensional shapes are proposed. Theoretical shapes are systematically compared with experimental shapes in order to discuss the adequacy of the proposed slowness surface. Part III presents photolithographic experiments made on silicon wafers of orientation $\{hk0\}$ and emphasis is placed on the lateral underetching and corner undercutting.

A three-dimensional graphical simulation of etched shapes relative to holes and mesa is derived starting from the dissolution slowness surface of silicon crystal. A comparison of theoretical and experimental shapes of etched structures is undertaken to define precisely the exact shape for the dissolution slowness surface.

2. Experimental procedure

Thin circular plates (1500 µm thick) were cut from a silicon ingot. The p-type material was normally in the

TABLE I Values for the angle of cut, φ_0, and identification of Miller indices for the corresponding $(h\,k\,l)$ plane in the vicinity of the reference surface. Only Miller indices smaller than 10 are indicated.

φ_0 (deg)											
0	5	10	14	18	23	26	30	34	37	42	45
hkl 010	–	$\bar{6}10$	$\bar{4}10$	$\bar{3}10$	$\bar{7}30$	$\bar{2}10$	$\bar{7}40$	$\bar{3}20$	$\bar{4}30$	$\bar{9}80$	$\bar{1}10$

range 0–30 Ω cm. Twelve orientations corresponding to $\{h\,k\,0\}$ planes were selected (Table I). The orientations were determined by using a double X-ray goniometer which offers an accuracy of about 30 s. Before etching, the planar surfaces and the circular contours of silicon plates were lapped with diamond abrasive and then optically polished.

A sulphuric acid–hydrogen peroxide mixture was used as a cleaning solution. The etchant was a concentrated (35%) KOH-wafer solution which is known to provide a high degree of anisotropy [10, 23, 24]. The silicon plates were treated with stirred KOH solutions at a constant temperature of 353 K in a oil-heated double-walled vessel. The temperature of the bath was controlled with an accuracy of $\pm\,0.5\,°C$.

After successive isothermal etchings the surface texture of etched silicon plates was characterized by means of two different procedures. First, the surface topography data were measured using a microcomputer-based mechanical surface profilometer. The diamond tip of the stylus has a finite size (about 2 μm). The digitalized surface profile is then numerically treated. The program offers, in particular, the possibility of extracting the distribution of slopes from the real profilometry trace as given by the stylus profilometer. Magnifications of surface profiles give important information on etched shapes. The etched surfaces were also examined by scanning electron microscopy using a relatively low accelerating voltage (typically 5 kV) and an observation angle of $0°$. The changes in shape of the starting circular $\{h\,k\,0\}$ sections were studied by using a Talyrond analyser, which generates the least square circle so that the out-of-roundness profiles of etched sections were displayed at relatively large magnifications with the superimposed reference circle.

Before and after etching thicknesses of etched plates were measured by means of a "Palmer" instrument which provides an accuracy of about 1 μm. At least five measurements were performed on each singly-rotated plate in order to evaluate an average value for the etch rate. Note also that the discrepancy between several measurements never exceeded 4 μm.

3. Experimental results
3.1. The orientation dependence of the etch rate
The plates of orientation $\{h\,k\,0\}$ investigated here correspond to plates cut parallel to the $[0\,0\,1]$ axis. The angle of cut, φ_0, i.e. the angle from the $(0\,1\,0)$ plane, lies in the range $0°–45°$. For a crystal belonging to the class $m3m$ the two faces of a singly rotated $\{h\,k\,0\}$ planes suffer similar chemical attacks. Then the etch rate, R, can be easily evaluated from the decre-
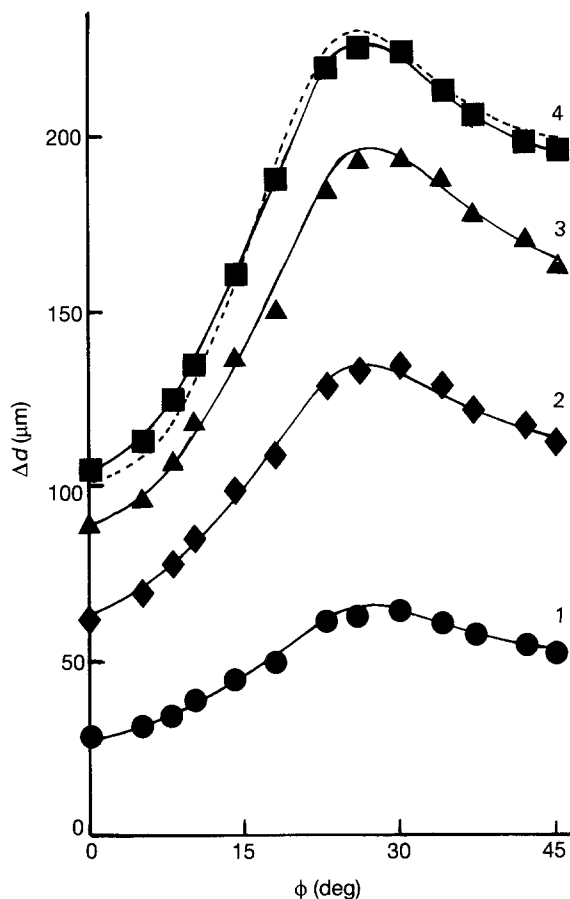

Figure 1 The decrement in thickness, Δd, against the angle of cut φ, for various conditions of chemical attack. (– – –) The theoretical variations ($t = 45$ min).

ment in thickness, Δd. Typical data relating the decrement in thickness as measured after several isothermal etchings to the angle of cut, φ_0, are plotted in Fig. 1. Curves 1–3 are, respectively, for one, two and three successive isothermal etchings corresponding to a time of 15 min. Curve 4 is for a single chemical attack of 45 min for which an additional inert gas purge was continuously applied. All the curves exhibit the same behaviour: the Δd versus φ_0 plots pass through a maximum for φ_0 in the vicinity of $26°$ (approximately for a $\{2\,1\,0\}$ plane) whereas minima in the etch rate occur for $\{0\,1\,0\}$ and $\{1\,1\,0\}$ planes. The dissolution rate of the $\{1\,0\,0\}$ surface is about 1.1 mm min^{-1}, whereas an etch rate ratio of about 1.85 is found for the $\{1\,1\,0\}/\{1\,0\,0\}$ planes. These results are in relative agreement with previously published data [10, 24].

### 3.2. Topology of etched surfaces
3.2.1. Surface profilometry traces
It is well known that an anisotropic chemical attack of crystal surfaces results in the formation of dissolution

figures whose geometrical features depend on the crystal orientation [1–3, 7, 44–48]. As a consequence, an etched surface profile exhibits a simple characteristic shape [2, 37, 43, 49]: convex or concave backgrounds, as well as dissolution profiles with alternate concave–convex or convex–concave shapes are frequently recognized. Moreover, according to the stability criteria discussed several years ago by Irving [2, 50], this characteristic shape does not vary with further etching even if, when a concave or a convex background develops, a prolonged chemical attack causes the rapid disappearance of surface elements with larger slopes.

For this reason, it is necessary to follow the changes in shape of etched surface profiles and in the corresponding distribution of slopes with the duration of etching, t. For this purpose, topography data were studied, which were obtained for two traces made along two perpendicular axes: one of these directions coincides with the direction X' obtained for the X axis ([1 0 0] axis) after the plates were singly rotated; the other trace corresponds to the [0 0 1] trace. Figs 2–7
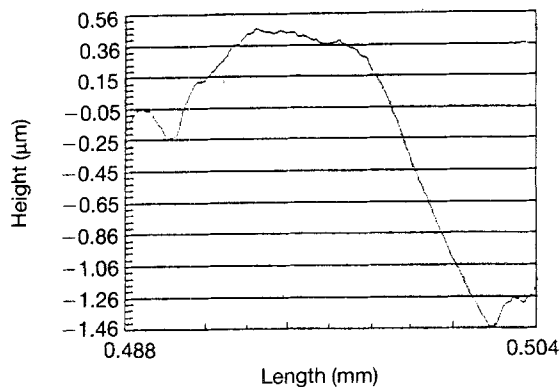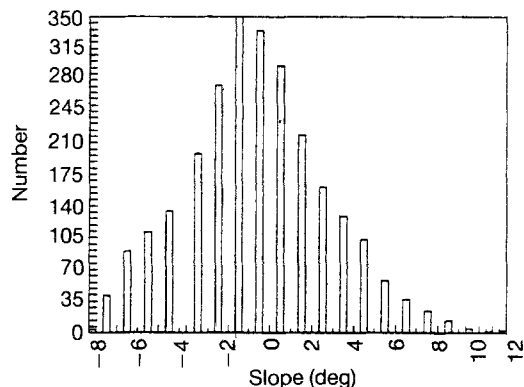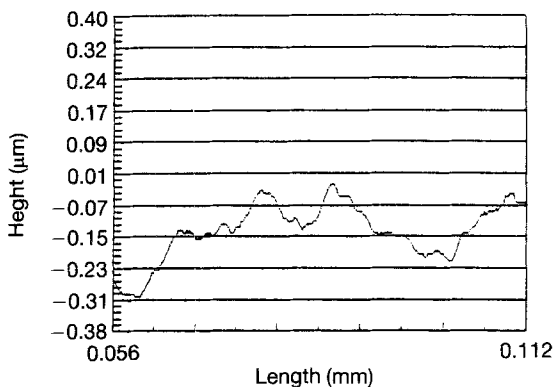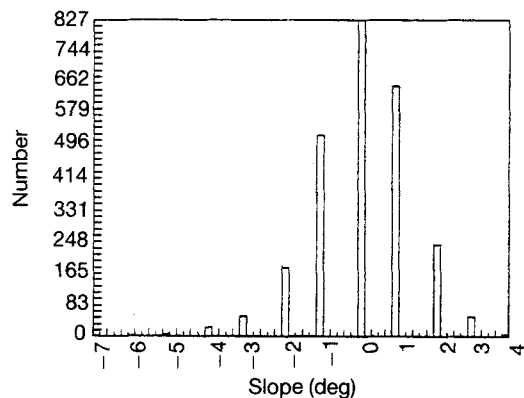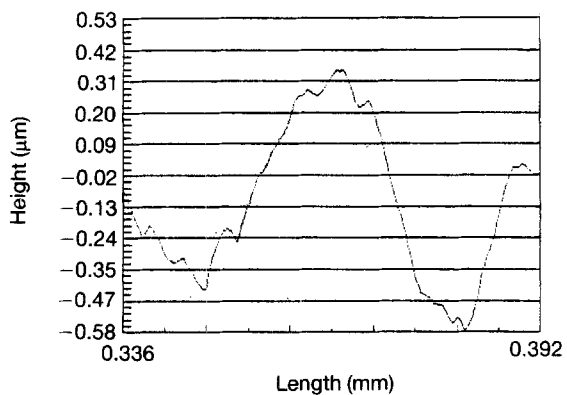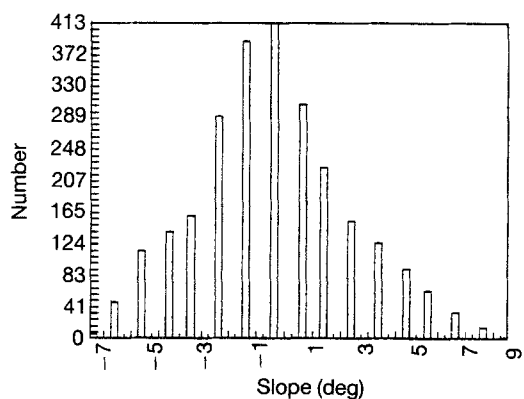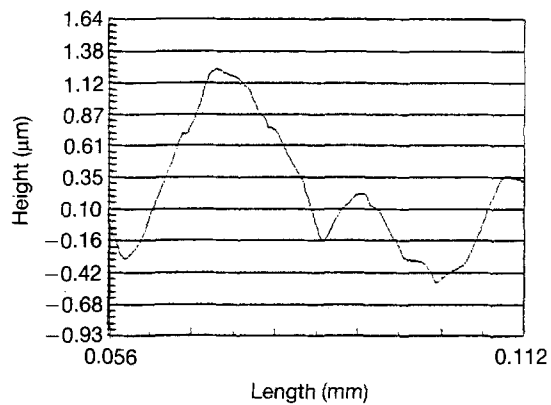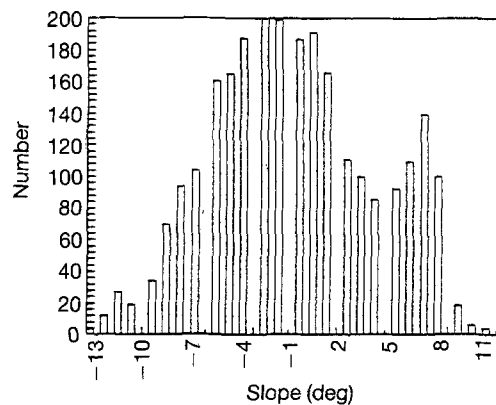
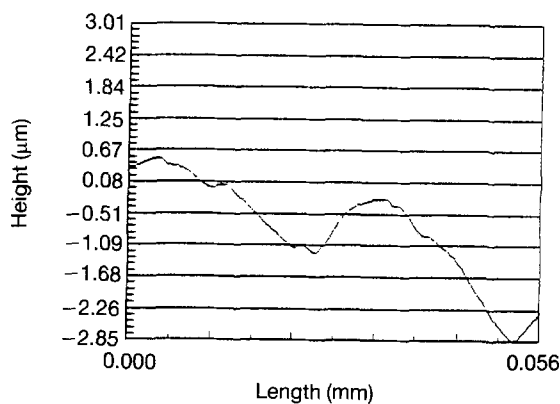

Figure 2 Changes with the etching time, t, in the profilometry traces and in the corresponding distributions of slopes. Traces are made along the X' axis of a (6 1 0) plate. (a, d) $t = 15$ min; (b, e) $t = 30$ min; (c, f) $t = 45$ min.
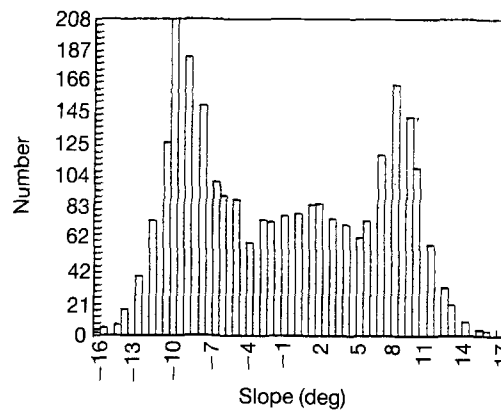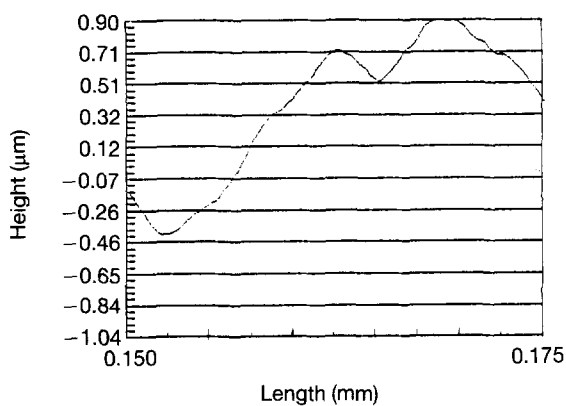
Figure 3 Changes with the etching time, *t*, in the profilometry traces and in the corresponding distributions of slopes. Traces are made along the X' axis of a ($\bar{3}$ 2 0) plate. (a, d) $t = 15$ min; (b, e) $t = 30$ min; (c, f) $t = 45$ min.
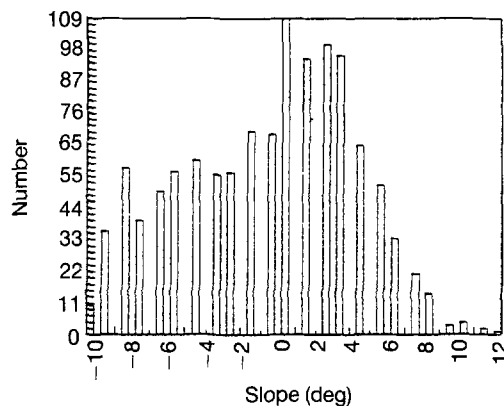
show the changes with etching time, *t*, in the shape of profilometry traces and in the corresponding distributions of the slopes. These figures reveal that the crystal orientation governs the development of dissolution surface profiles and that the stability criteria are effectively verified for the anisotropic dissolution of silicon crystals in KOH etchant. In particular, if the etching time, *t*, reaches 15 min, we can identify easily the characteristic shape of the various profilometry traces. Moreover, the distributions of slopes reflect the geo-

metrical features of profilometry traces. Symmetrical distributions are associated with a convex (Fig. 5) or a concave (Fig. 4) background; in addition, such distributions show decreasing slopes with increasing etching times (see Fig. 5, for example). Negatively or positively skewed slope distributions, together with a spread which extends asymmetrically to large angles (Figs 2 and 3), are related to traces with alternate shapes. Very large spreads in the distribution of slopes (Figs 6 and 7) are correlated to the development of
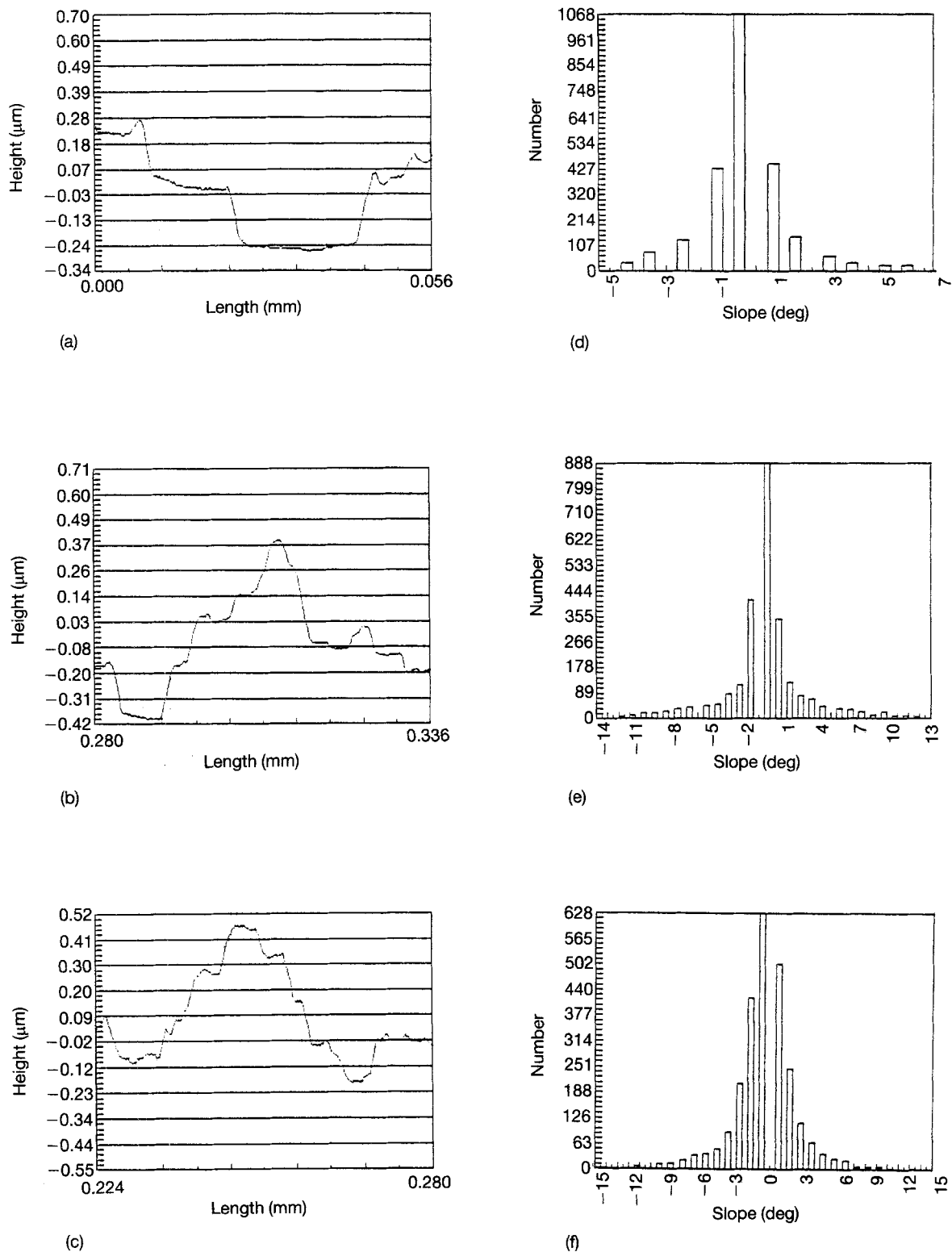
5956

Figure 4 Changes with the etching time, t, in the profilometry traces and in the corresponding distributions of slopes. Traces are made along the X' axis of a $(\bar{1}\,1\,0)$ plate. (a, d) $t = 15$ min; (b, e) $t = 30$ min; (c, f) $t = 45$ min.

surface profiles composed of elements whose slopes remain unaltered on prolonged etching.

Because the dissolution process is essentially determined by the orientation of crystal surfaces, we can conveniently concentrate our attention on the final X' and [0 0 1] profilometry traces which are collected in Figs 8 and 9. Three interesting features emerge from these figures.

(i) Let us turn our attention to the directional effects one may observe in profiles. The characteristic shape of X' traces clearly shows a continuous evolution as the angle of cut, φ_0, varies from $0°$–$45°$. The shape changes successively from concave ($\varphi_0 = 0°$, Fig. 8a) to convex–concave ($\varphi_0 = 5°$–$18°$) and from convex ($\varphi_0 = 23°$, Fig. 8f) to concave–convex ($\varphi_0 = 30°$–$42°$), finally reaching for $\varphi_0 = 45°$ (Fig. 8c) a stable rather concave background. From Fig. 1 one can see that, as expected, a concave (or a convex) background is formed when a minimum (or a maximum) of the etch rate occurs for an orientation
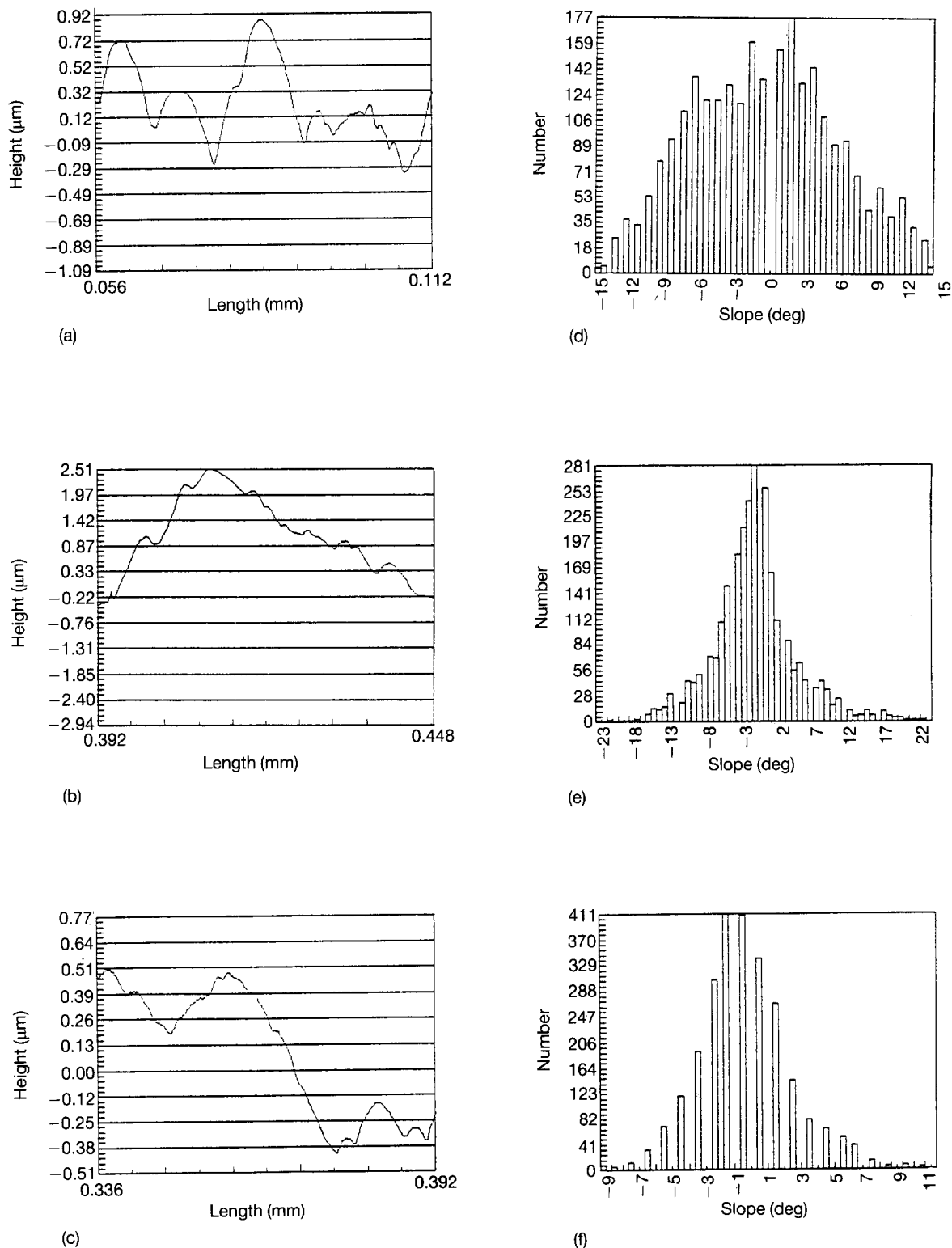
Figure 5 Changes with the etching time, t, in the profilometry traces and in the corresponding distributions of slopes. Traces are made along the [0 0 1] axis of a ($\overline{6}$ 1 0) plate. (a, d) $t = 15$ min; (b, e) $t = 30$ min; (c, f) $t = 45$ min.

corresponding to that of the reference crystal surface.

(ii) The [0 0 1] profilometry traces either of convex (Fig. 9c–e) or concave (Fig. 9a, b) nature can be qualified as "symmetrical backgrounds". The symmetrical nature of the profile shapes is simply connected to the symmetry properties of class $m3m$. Effectively one must take into account that the (0 0 1) plane lies perpendicular to the direction of traces.

(iii) It should also be noticed that the shape of [0 0 1] profiles remains very sensitive to small angular

misorientations for ϕ_0 around 0° and 45°. We observe that small changes in the angle of cut produce a rapid modification of the profile shape from concave to convex for ϕ_0 in the vicinity of 0° (Fig. 9a, b) or from convex to concave for a misorientation of 3° from a {1 1 0} plane (Fig. 9k, l).

3.2.2. Scanning electron microscopy

The scanning electron micrographs shown in Figs 10 and 11 illustrate very well the stability criteria formulated by Irving. As soon as the duration of etching
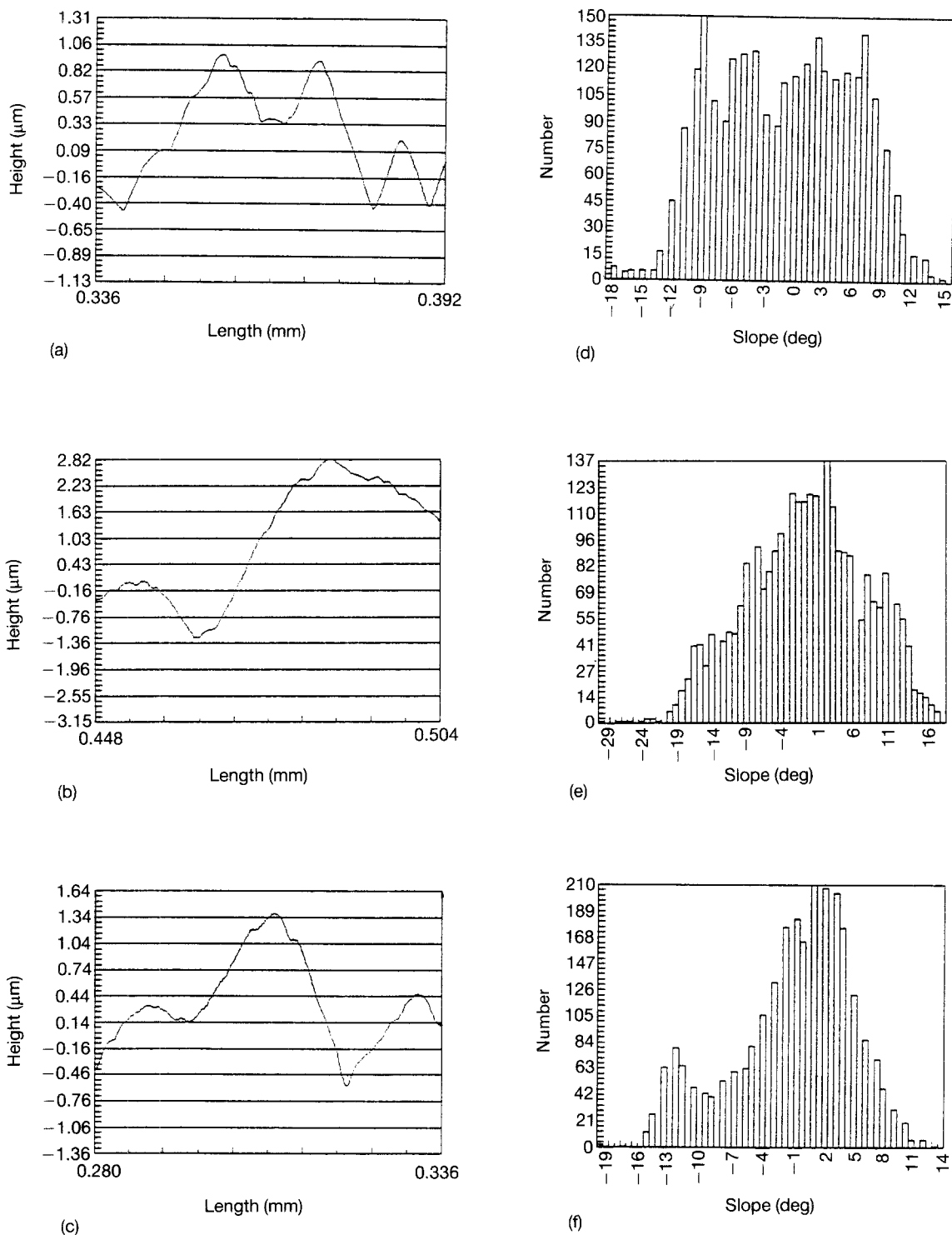
Figure 6 Changes with the etching time, *t*, in the profilometry traces and in the corresponding distributions of slopes. Traces are made along the [0 0 1] axis of a ($\bar{3}$ 2 0) plate. (a, d) *t* = 15 min; (b, e) *t* = 30 min; (c, f) *t* = 45 min.

exceeds a critical time (estimated to be about 15 min), characteristic pits or hillocks develop whose shape is only determined by the orientation of the surface on which they are formed.

Repeated etchings do not modify the shape of the dissolution figures but only produce an enlargement of pits or hillocks (Fig. 11, for example) for some specific (*h* *k* 0) orientations. This behaviour agrees well with previous works on the dissolution of quartz crystals in $NH_4F \cdot HF$ solutions [5, 7, 37, 46, 47] or of silicon crystals in EDP etchant [24, 45].

Scanning electron micrographs showing the final texture of the various etched (*h* *k* 0) surfaces are collec-

ted in Fig. 12a–l. These micrographs allow us to describe schematically in Table II the specific etch figures relative to (*h* *k* 0) planes. The final scanning electron micrographs as well as Table II confirm the preceding remarks (i–iii) which were formulated after studying orientation effects in profilometry traces.

3.3. Out-of-roundness profiles as a function of crystal orientation

Here again it is necessary to verify the stability criteria by following the evolution of out-of-roundness profiles related to various cross-sections with the etching
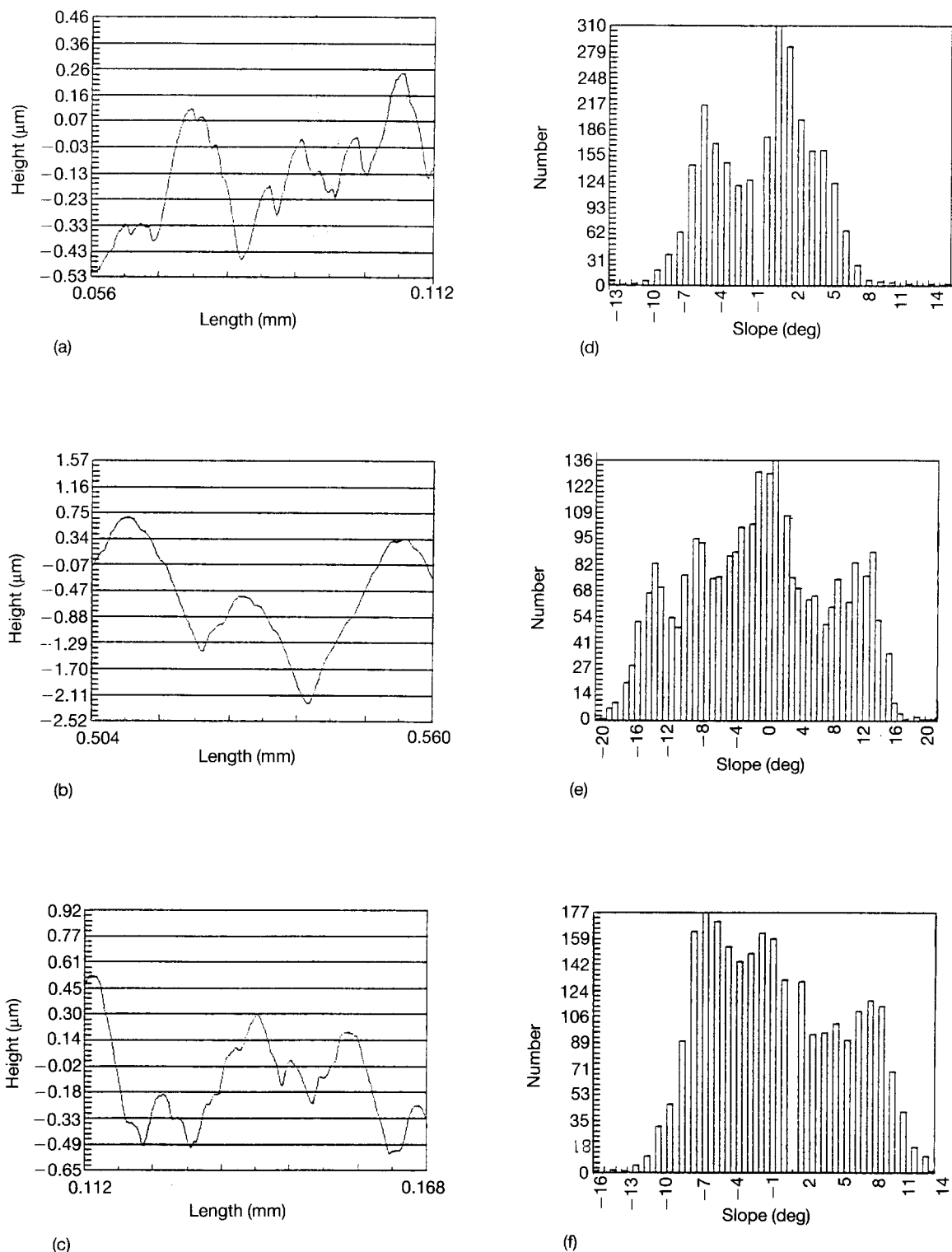
5959

Figure 7 Changes with the etching time, t, in the profilometry traces and in the corresponding distributions of slopes. Traces are made along the [0 0 1] axis of a ($\bar{1}$ 1 0) plate. (a, d) t = 15 min; (b, e) t = 30 min; (c, f) t = 45 min.

time, t. After a critical etching time of about 15 min, a visual inspection (Figs 13 and 14) of cross-sectional out-of-roundness profiles reveals the formation of peaks and valleys which, in theory [42, 43], are respectively connected with maxima and minima in the dissolution slowness. In reality, the maxima and minima in the out-of-roundness profiles correspond to specific directions lying in the $\{hk0\}$ plane which make an angle θ_e with the X' axis. With prolonged etching, maxima in the out-of-roundness profiles become more peaky, some valleys (V_1 in Fig. 13d, for

example) tend to flatten, whereas some minor peaks and valleys (p_1 and V_1 in Fig. 13c) develop as the etching time reaches 45 min. However, the major fact is that, at first sight, the angular position of extrema remains unchanged with repeated isothermal etchings. This observation is confirmed by examination of Table III which shows the evolution of the angular position, θ_e, of extrema with the etching time, t. Deviations of less than 3° are found, even for angular positions, θ_M, of peaks. The quasi-stability of angles, θ_m, is not surprising because the bottoms of valleys are

5960

just produced by minima in L connected with limiting facets [42, 43]. The fact that the angular position, θ_M, of peaky maxima seems insensitive to the duration of etching can be attributed to the existence of symmetrical portions of the polar graph in the neighbourhood of maxima for L.

Because the stability criteria are verified again here, we can illustrate the orientation effect in dissolution profiles by means of Fig. 15, which represents the final out-of-roundness profiles related to $(hk0)$ sections. The results shown in Fig. 15 suggest several points.

1. A KOH solution etches initially circular sections according to the symmetry operations specific to class $m3m$. The (010) out-of-roundness profile shows clearly a four-fold symmetry about the $[010]$ axis. For the other $\{hk0\}$ etched profile graphs, it is sufficient, as expected, to cover a sector of $90°$ extending from the Z-axis to the X'-axis to characterize completely the orientation effect.

2. The decrement in diameter, $\Delta\Phi$, measured along the $[001]$ axis does not depend on the angle of cut, φ, because the (001) plane is tangential to the various
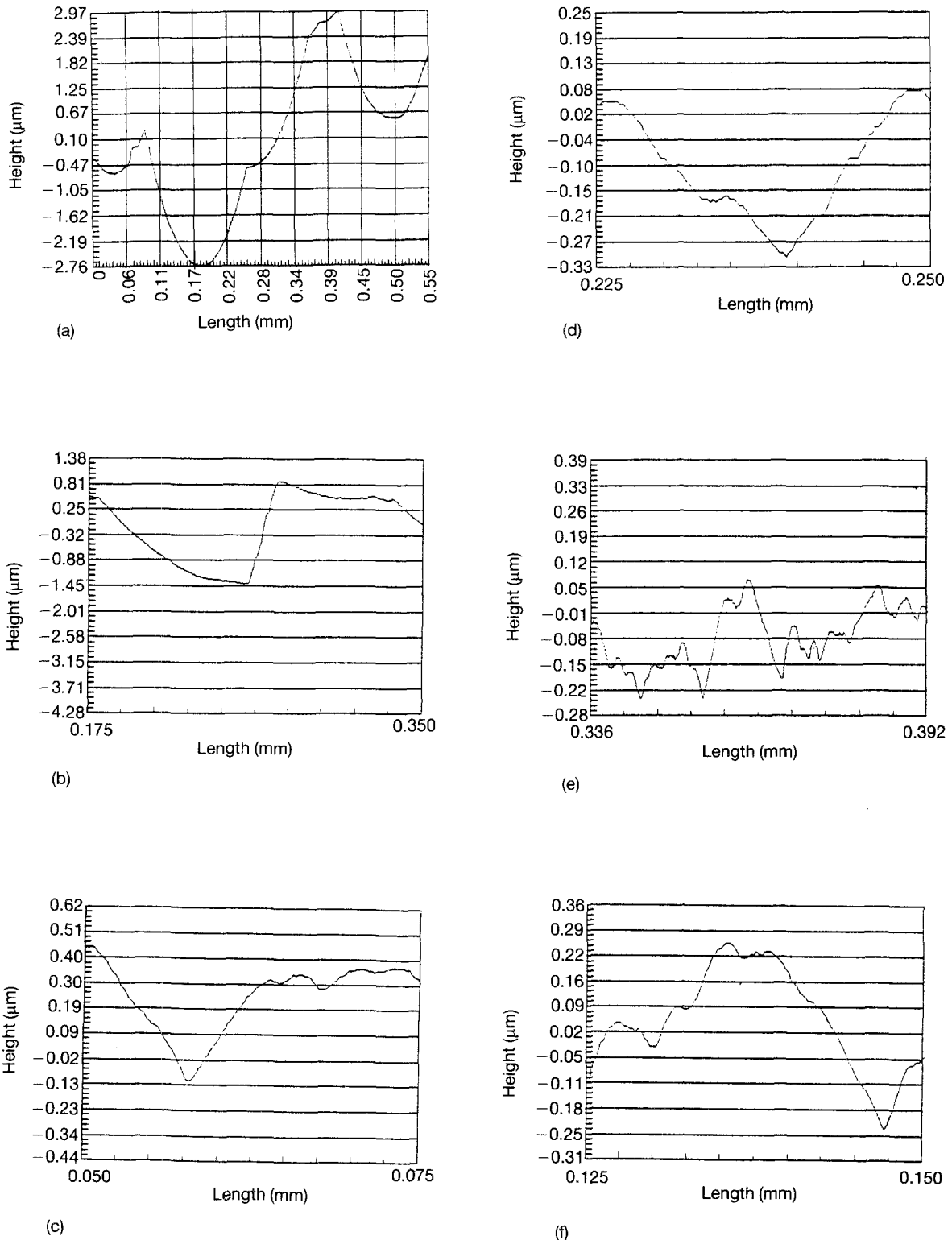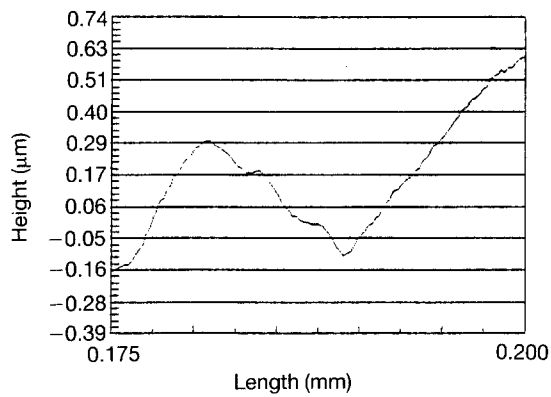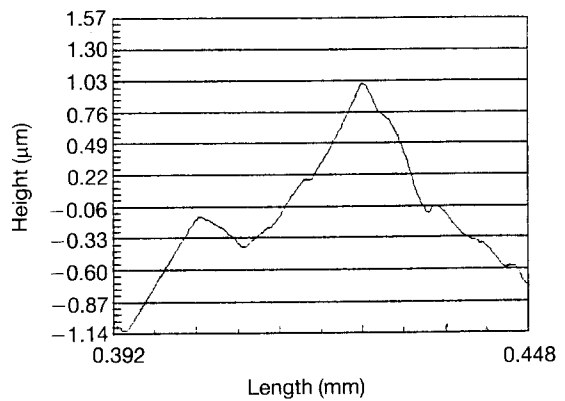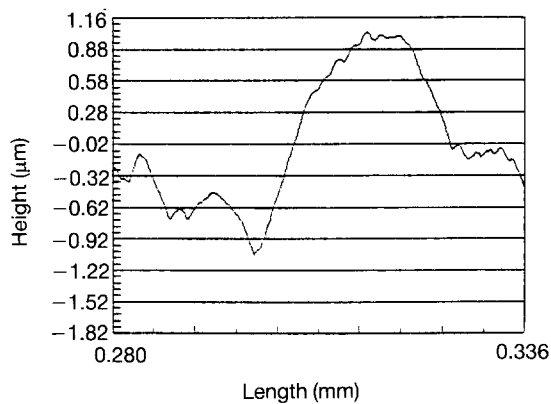

Figure 8 Changes in the final X', profilometry traces with the angle of cut, φ: (a–l) $\varphi = 0°$, $5°$, $10°$, $14°$, $18°$, $23°$, $26°$, $30°$, $34°$, $37°$, $42°$ and $45°$, respectively.
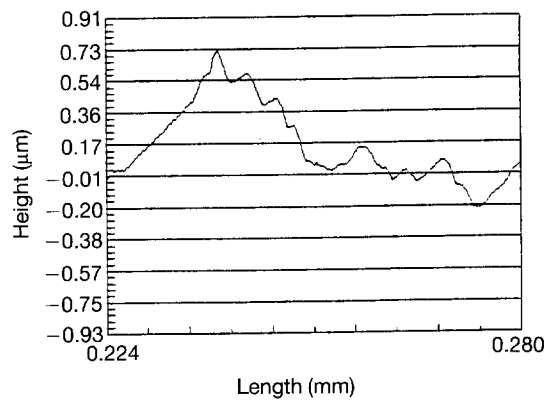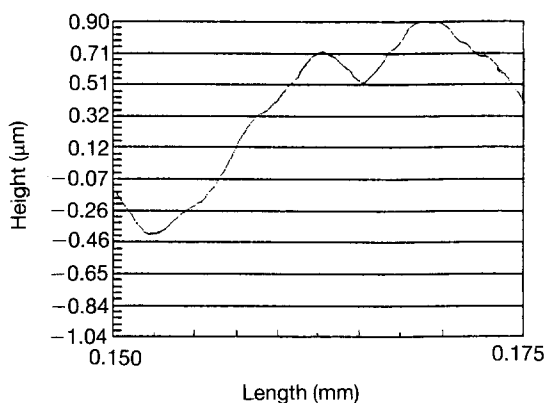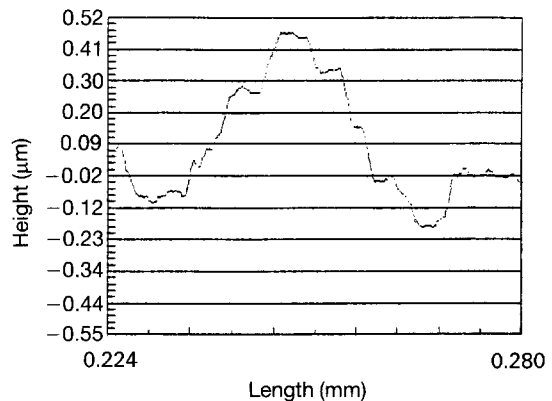
Figure 8 (continued).

{hk0} cross-sections. Moreover, on examining carefully Fig. 15a and Table III one can see that for an etched (0 1 0) section the final magnified out-of-roundness profile resembles the reciprocal of the etch rate versus φ plot presented in Fig. 1. In particular, angular positions of extrema, θ_e, in the out-of-roundness profile (or in a ΔΦ versus θ plot) coincide exactly with those, φ_e (or θ_e), which occur in the R^{-1} versus φ (or versus θ) plot describing the orientation dependence of the etch rate, R, for singly-rotated silicon plates.

3. The out-of-roundness profiles displayed in Fig. 15 show continuous and progressive changes in shape with the angle of cut, φ. The section with φ = 14° exhibits the more complicated shape with the formation of minor extrema m_1 and M_1 (Fig. 15d). As the angle of cut reaches 26° we observe the development of an accentuated peak, M_2, (Fig. 15g) for θ_M in the vicinity of 36°. This behaviour can be attributed to the early influence of {1 1 1} planes which dissolve very slowly [10, 24, 44]. As can be seen from Table IV,

which gives the final angular positions of extrema in the out-of-roundness profiles, the etched (1 1 0) profile graph presents effectively a pronounced maximum for a direction ($\theta_e \approx 36°$) which coincides with the [1 1 1] axis.

4. Determination of the dissolution slowness surface

4.1. Definition of a procedure

In a previous paper [41], we have proposed a generalized equation to express the dissolution slowness, $L(\varphi, \theta)$ of a cubic crystal belonging to class 23. This equation has been derived in the framework of the tensorial model for the anisotropic etching of crystals. Rules to simplify this equation when we are concerned with other cubic classes have been also given. Applying these rules to the class $m\,3\,m$ we obtain
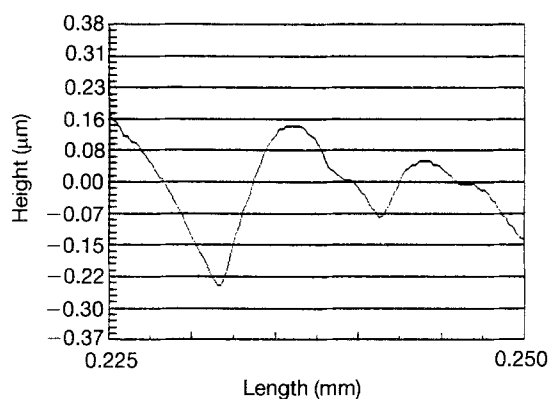
$$L(\varphi, \theta) = S_1^* + S_2^* \tag{1}$$

with
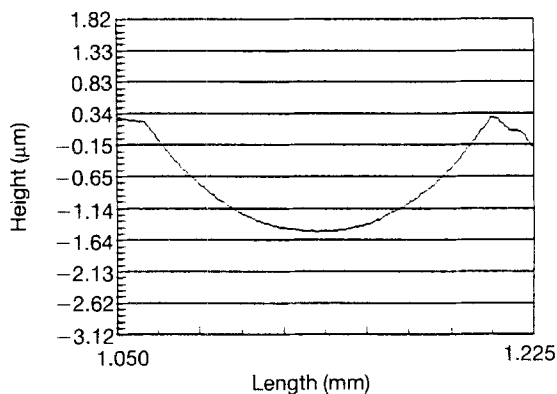
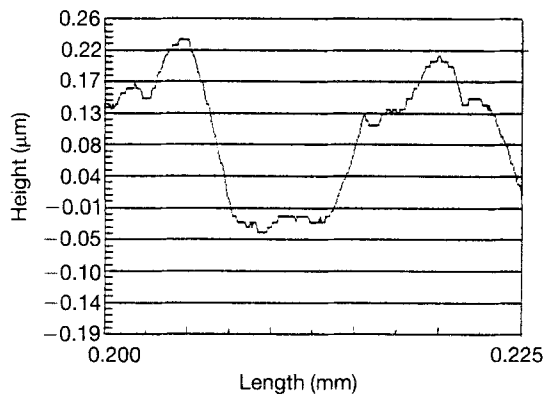$$S_1^* = \sum_{k=0} a_k^* (\cos\theta, \sin\theta)^{2k} \tag{2}$$
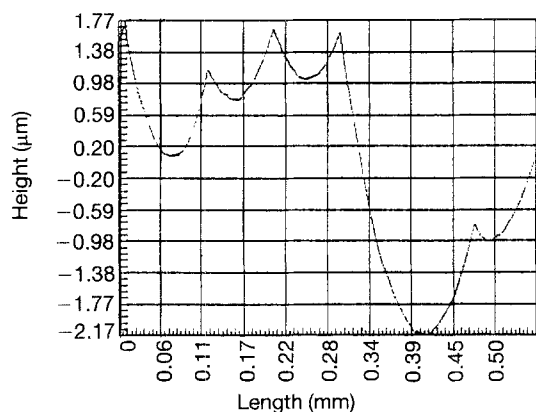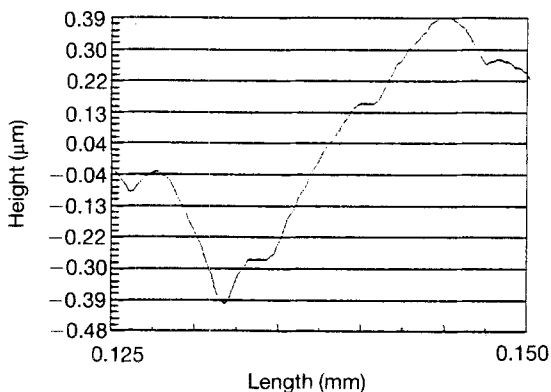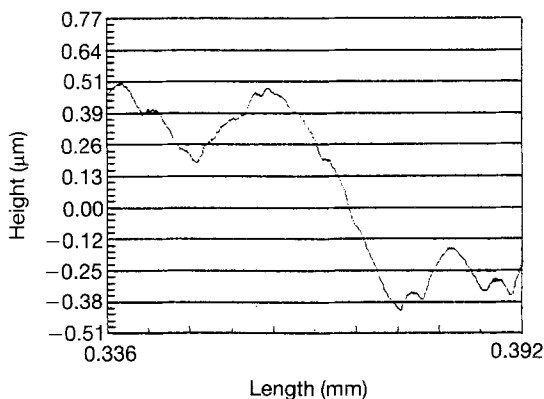
Figure 9 Changes in the final [0 0 1] profilometry traces with the angle of cut, φ: (a–l) $\varphi = 0°$, $5°$, $10°$, $14°$, $18°$, $23°$, $26°$, $30°$, $34°$, $37°$, $42°$ and $45°$, respectively.
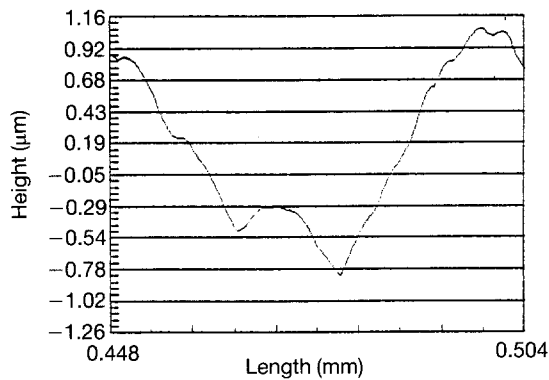
(g)
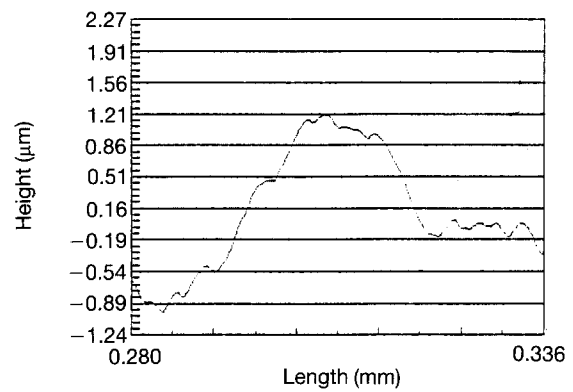
(j)
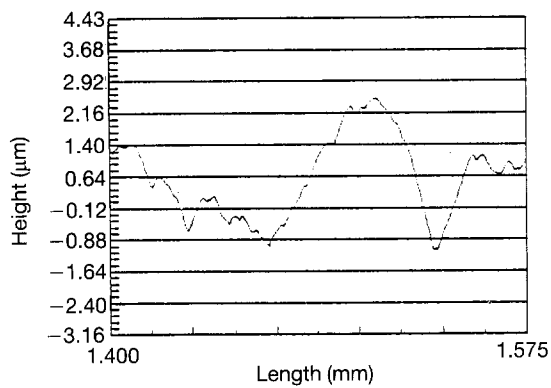
(h)
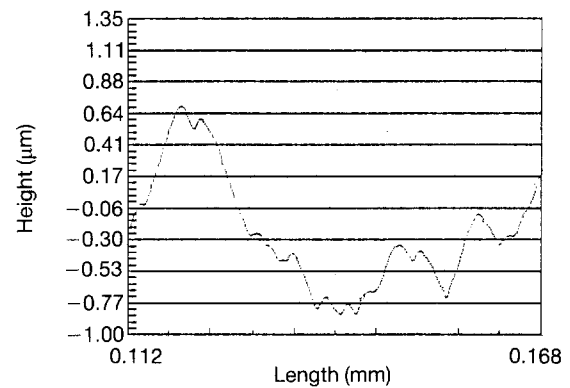
(k)
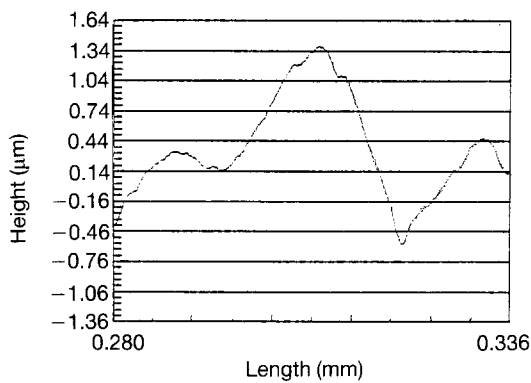
(i)
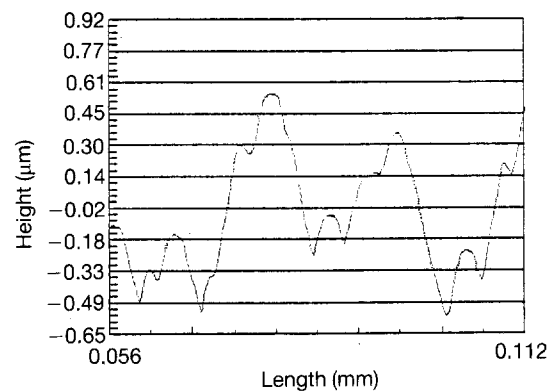
(l)

Figure 9 (continued).

$$S_2^* = \sum_{l=1} \sum_{m=0} b_{l,m}^* (\sin \varphi \cos \varphi \cos{}^2\theta)^{2l} (\cos \theta)^{2m}$$

(3)

where φ and θ are the angles of cut as defined by the IEEE Standards [51].

The coefficients of series, a_k^* and b_{lm}^* appearing in Equations 1 and 2 are expressed in terms of the independent dissolution constants of tensors. In the general equation we are concerned with dissolution tensors whose ranks vary from $0-N_{max}$. Depending on the values for N_{max}, the subscripts k, l and m must, in

addition, obey the following selection rules [41]: $4k \leqslant N_{max}$, $4l + 2 \leqslant N_{max}$.

When φ and θ vary, the vector L describes in space a representative surface called the dissolution slowness surface. The complexity of the dissolution slowness surface, specially the number of extrema, is directly connected to the maximum rank, N_{max}.

It is obvious that the dissolution constants involved in the coefficients of series must be determined from experiments. If, after analysing data, one expects that the slowness surface will exhibit a relatively simple shape, the rank N_{max} can be limited to $N_{max} = 10$.
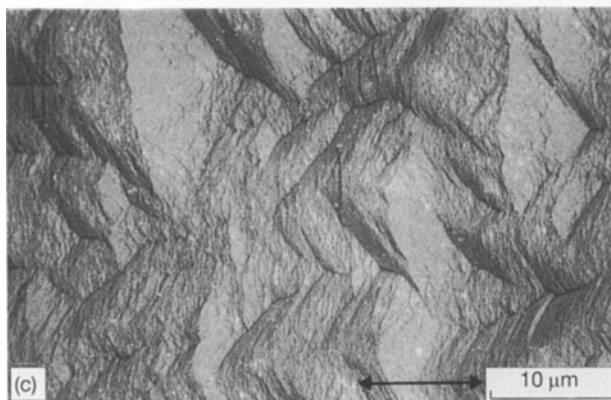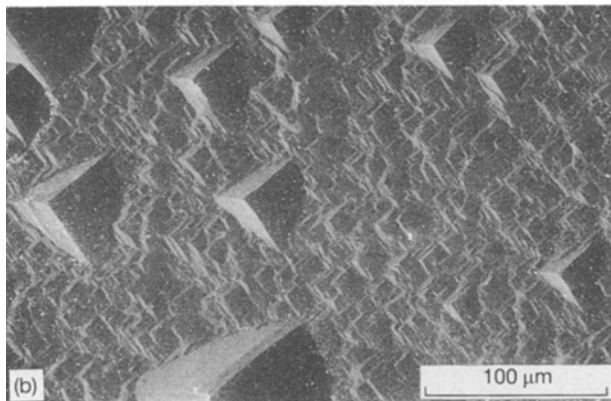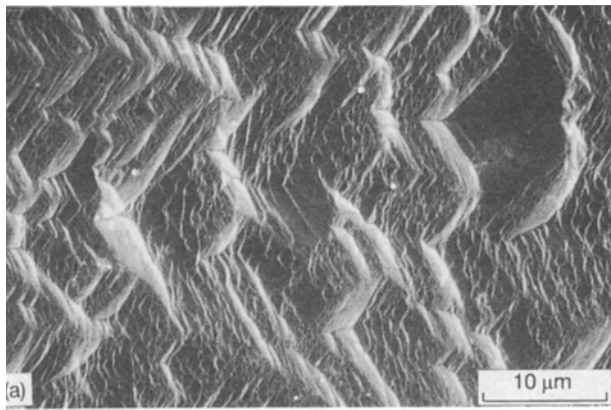
Figure 10 Changes, with the etching time, t, in the surface texture of an etched $(\bar{6}\,1\,0)$ plate. $t =$ (a) 15, (b) 30 and (c) 45 min.
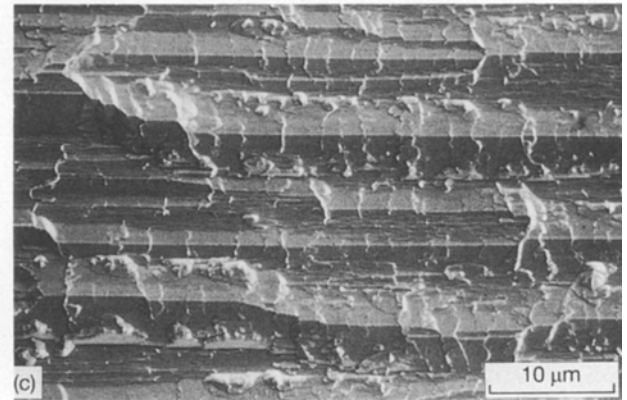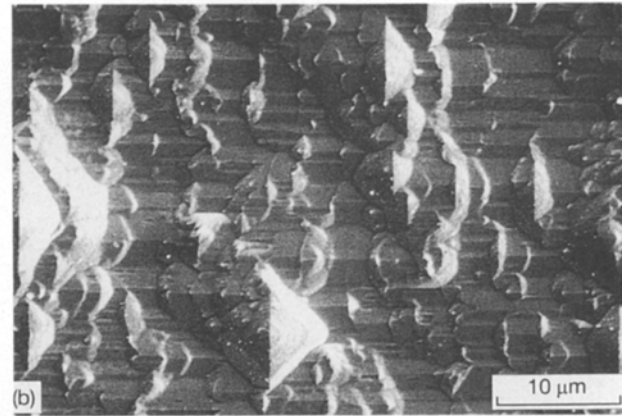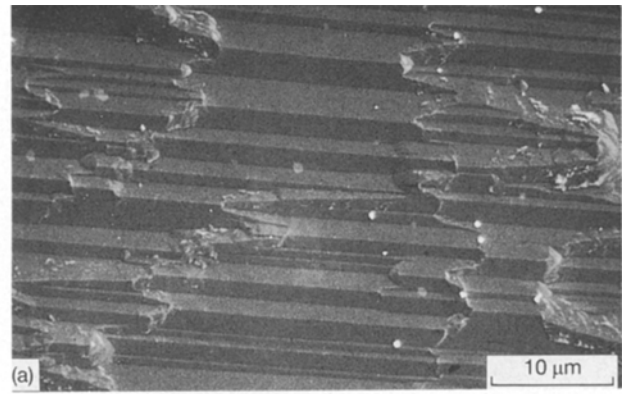
Figure 11 Changes, with the etching time t, in the surface texture of an etched $(\bar{1}\,1\,0)$ plate. $t =$ (a) 15, (b) 30 and (c) 45 min.

TABLE II Geometrical features of final etching patterns ($t = 45$ min) as revealed by SEM examination

Angle of cut, φ_0 (deg)	Geometrical features as viewed on scanning electron micrographs
0	Flat pits fitted into each other
5	Terraced pits with flat bottom
10	Features similar to those related to $\varphi_0 = 5°$ but in addition dissolution figures overlap
14	Steady hillocks aligned along the X'-axis, fitted into each other and presenting striations arranged along the $[0\,0\,1]$ axis
18	Bumpy surface composed of numerous folds aligned the $[0\,0\,1]$ axis
23	Features close to those related to $\varphi_0 = 18°$
26	Features similar to those related to $\varphi_0 = 23°$, however, the rather elongated hillocks seem to be bounded by two small facets
30	Bumpy hillocks whose sides are composed of limiting facets. Striations along the $[0\,0\,1]$ axis are still present
34	Features similar to these related to $\varphi_0 = 30°$ with a predominance of facets
37	Elongated "bumps" bounded by facets. The direction of alignment correspond to the X'-axis
42	Linearly textured surface with elongated "pits" aligned along the X'-axis
45	Linearly textured surface composed of grooves arranged along the X'-axis

Then, if we make use of all tensors whose ranks lie in the range [0, 10], we have to estimate 16 dissolution constants. But if one suspects the surface to possess a large number of extrema, it can become necessary to work with tensors corresponding to $N_{max} = 18$. In this case, the total number of dissolution constants reaches 37. As a result, the adjustment of the various dissolution constants becomes a very difficult task.

Thus, when we turn to the problem of determining the dissolution constants which appear in the analytical equation of the representative surface of the dissolution slowness, we have to answer a fundamental

Figure 12 Final scanning electron micrographs for differently-oriented $(h k 0)$ plates. (a–l) $\varphi = 0°$, $5°$, $14°$, $23°$, $26°$, $30°$, $34°$, $37°$, and $42°$, respectively. Direction of alignment of the X' axis is indicated on the micrographs.

Figure 12 (continued).

Figure 13 Changes in the out-of-roundness profiles with the etching time, t, for cases where $\varphi = 14°$ (a–c) and $\varphi = 23°$ (d–f). (a, d) $t = 15$ min; (b, e) $t = 30$ min; (c, f) $t = 45$ min.
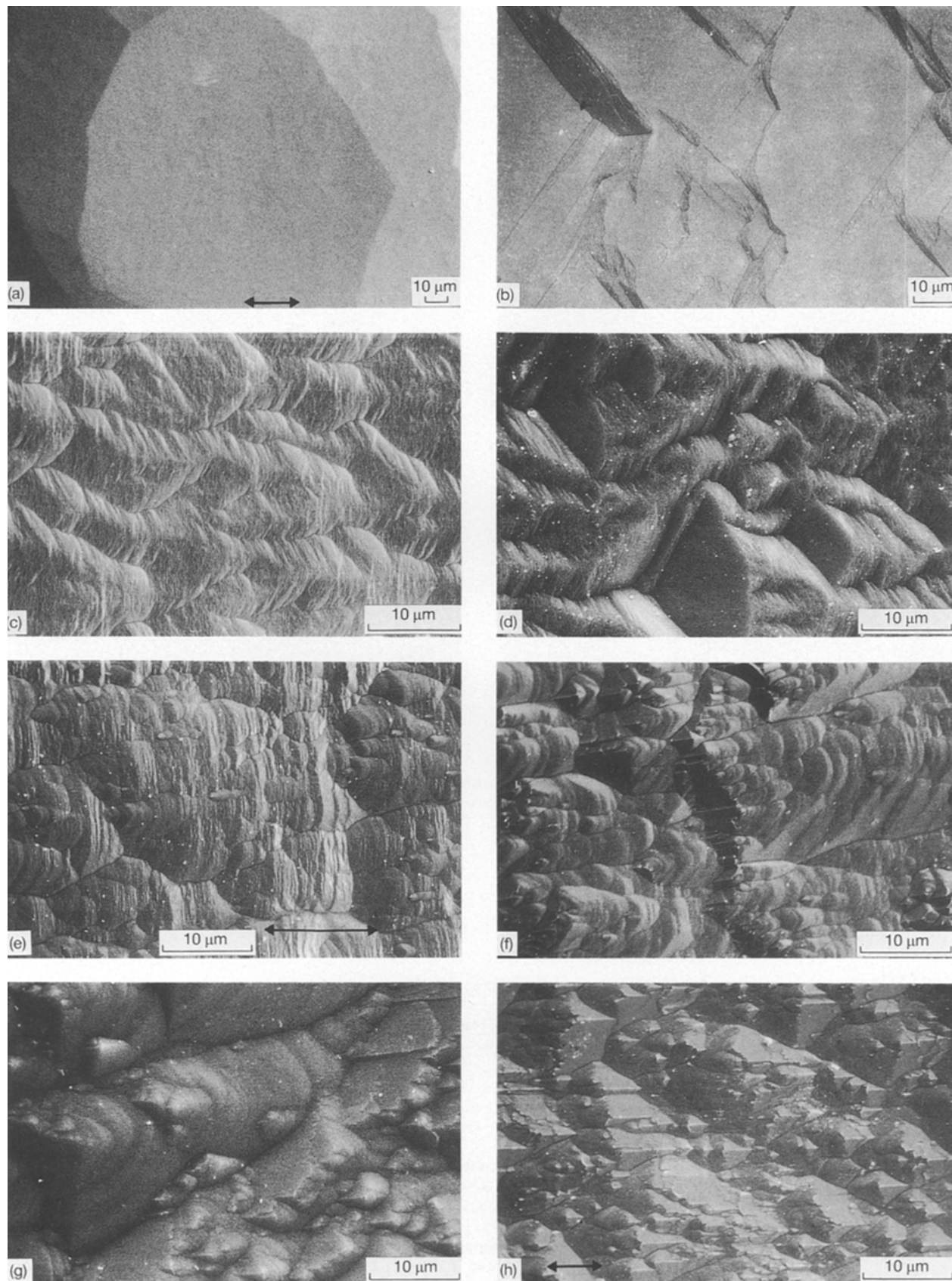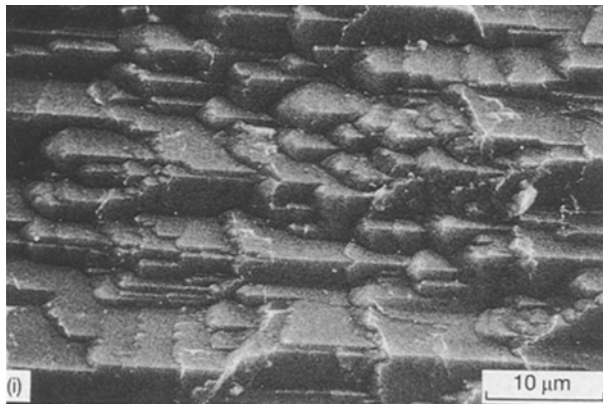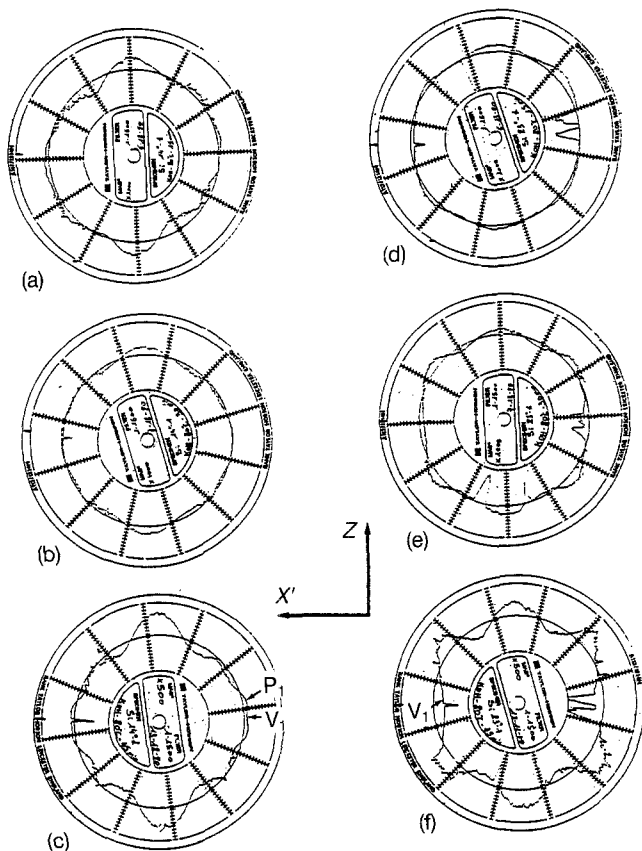

Figure 14 Changes in the out-of-roundness profiles with the etching time, t, for cases where $\varphi = 34°$ (a–c) and $\varphi = 45°$ (d–f). (a, d) $t = 15$ min; (b, e) $t = 30$ min; (c, f) $t = 45$ min.

question: is it necessary to work with all the dissolution constants of tensors ranging from rank 0 to maximum rank N_{max}? The answer is no. Effectively, Tellier and co-workers have shown that, as the rank N_{max} increases, the slowness surface exhibits a more and more complex shape characterized by an increasing number of extrema. Then it is sufficient to determine only dissolution constants involved in tensors of higher ranks to obtain a slowness surface which describes conveniently the anisotropic dissolution process. In reality, for the etching process of KOH on silicon crystals, we have evaluated dissolution constants related to tensors of rank 16–18 (Table V).

Care must be taken that with this simplified procedure the coefficients of series take non-zero values so

that Equations 1–3 still remain valid. However, equations expressing a_k^* and $b_{l,m}^*$ now involve a reduced number of dissolution constants. For example, coefficients a_1^* and $b_{1,1}^*$ involve now 4 and 10 constants, respectively, instead of the respective 17 and 25 dissolution constants introduced in the general procedure.

In practice, the experimental determination of dissolution constants involves the analysis of several types of data, namely,

(i) the etch rate versus orientation plot related to singly rotated silicon plates;

(ii) the changes in shape with orientation (φ, θ) and with direction of traces for surface profilometry traces;

(iii) the evolution in shape with angles of cut for out-of-roundness profiles.

This determination is based on several theoretical observations and features [42, 43]. These features, which establish a correlation between the morphology of the dissolution slowness surface and theoretical etched shapes, can be summarized as follows [42, 43, 52].

1. An out-of-roundness profile constitutes a crude "image" of the polar diagram for L in the corresponding cross-sectional plane.

2. From the out-of-roundness profile of an initially cylindrical crystal, we deduce the exact orientations (φ_m, θ_m) connected to minima in L. Moreover, in general, we recognize crudely the orientations (φ_M, θ_M) associated to maxima in L (for silicon the deviations are in practice estimated to be less than $\pm 3°$).

TABLE III Changes, with the etching time, t, in the angular position for successive extrema in various out-of-roundness profiles. Corresponding decrements in diameter, $\Delta\Phi$, are also indicated for $t = 45$ min. φ_0 is the angle of cut. Subscripts m and M correspond to a minimum (valley) and to a maximum (peak), respectively.

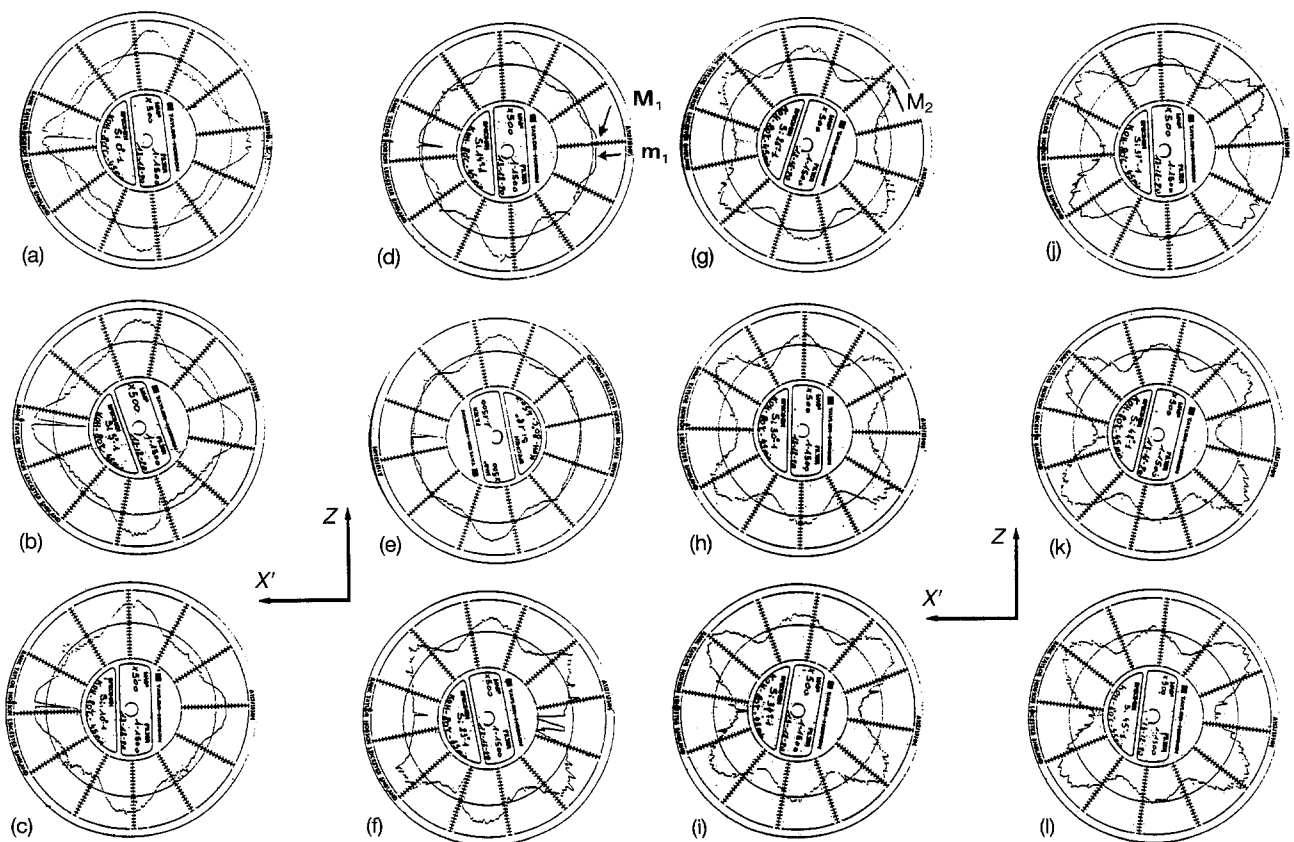| φ_0 (deg)	θ_e (deg)						
	θ_m	θ_M	θ_m	θ_M	θ_m	θ_M	t (min)
		0	27	45	63	90	15
0		0	25	45	64	90	30
		0	27	45	63	90	45
$\Delta\Phi$ (μm)		100	179	169*	180	100	45
		0	19	42	53	90	15
10		0	27	44	63	90	30
		0	28	45	64	90	45
$\Delta\Phi$ (μm)		118	169	147	170	103	45
			22	42	67	90	15
14			25	44	63	90	30
	0	10	27	43	63	90	45
$\Delta\Phi$ (μm)	140		164	148	177	100	45
	0			39	62	90	15
23	0			39	62	90	30
	0			40	63	90	45
$\Delta\Phi$ (μm)	172			98	163	103	45
	0			36	63	90	15
34	0			35	63	90	30
	0			37	63	90	45
$\Delta\Phi$ (μm)	177			65	162	110	45
	0			37	65	90	15
45	0			36	63	90	30
	0			36	64	90	45
$\Delta\Phi$ (μm)	166*			43	139	101	45

Figure 15 Orientation effect in the final out-of-roundness profiles related to various singly-rotated silicon plates. (a–l) $\varphi = 0°$, $5°$, $10°$, $14°$, $18°$, $23°$, $26°$, $30°$, $34°$, $37°$, $42°$, and $45°$, respectively.

TABLE IV Final ($t = 45$ min) angular positions for the successive extrema in the various out-of-roundness profiles relative to differently-oriented silicon plates (angle of cut φ_0)

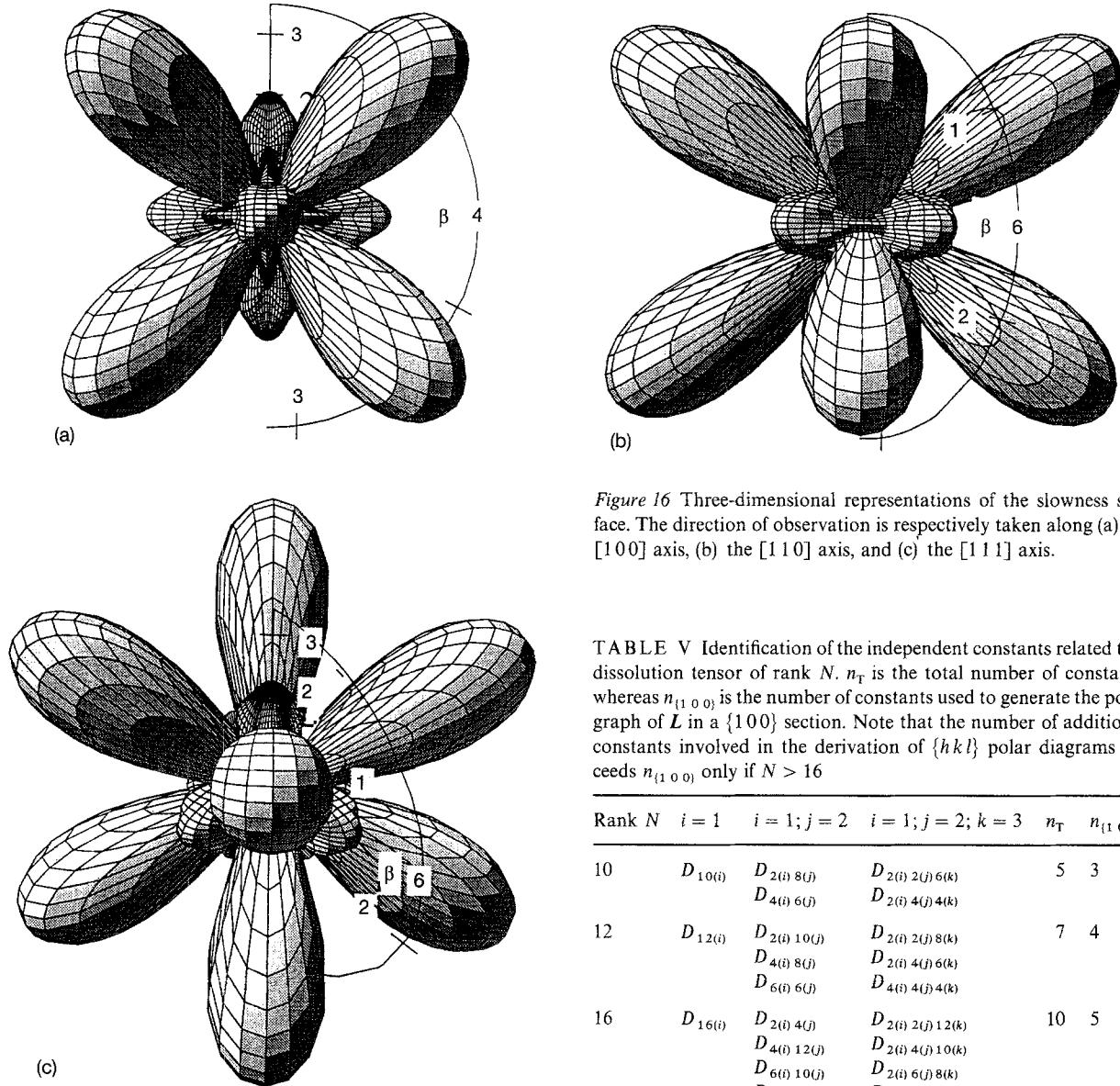|	φ_0 (deg)											
	0	5	10	14	18	23	26	30	34	37	42	45
θ_e (deg): Maxima	0, 45, 90	0, 45, 90	0?, 45, 90	10, 43, 90	12, 41, 90	40, 90	36, 90	37, 90	37, 90	34, 90	35, 90	36, 90
Minima	27, 63	28, 62	28, 64	0, 27, 63	0, 23, 62	0, 63	0, 63	0, 64	0, 63	0, 61	0, 62	0, 64

(a)

(b)

(c)

Figure 16 Three-dimensional representations of the slowness surface. The direction of observation is respectively taken along (a) the [1 0 0] axis, (b) the [1 1 0] axis, and (c) the [1 1 1] axis.

3. Examination of the etched shape of surface profiles gives additional possibilities, such as an easy verification of the orientation (φ_e, θ_e) for extreme in L and an opportunity to detect the presence of a minor extremum in the vicinity of the orientation (φ_0, θ_0) of the reference surface.

We have made use of all these possibilities to propose a complete procedure to generate the dissolution slowness surface of silicon crystal. This procedure consists of [52]:

(a) generating by iterations the slowness surface until, in a first step, the (0 0 1) polar diagram of L fits very well the experimental L versus φ plot and, in the second step, theoretical (h k 0) polar diagrams resem-

TABLE V Identification of the independent constants related to a dissolution tensor of rank N. n_T is the total number of constants, whereas $n_{\{1\,0\,0\}}$ is the number of constants used to generate the polar graph of L in a $\{1\,0\,0\}$ section. Note that the number of additional constants involved in the derivation of $\{h\,k\,l\}$ polar diagrams exceeds $n_{\{1\,0\,0\}}$ only if $N > 16$

Rank N	$i = 1$	$i = 1; j = 2$	$i = 1; j = 2; k = 3$	n_T	$n_{\{1\,0\,0\}}$
10	$D_{10(i)}$	$D_{2(i)\,8(j)}$ $D_{4(i)\,6(j)}$	$D_{2(i)\,2(j)\,6(k)}$ $D_{2(i)\,4(j)\,4(k)}$	5	3
12	$D_{12(i)}$	$D_{2(i)\,10(j)}$ $D_{4(i)\,8(j)}$ $D_{6(i)\,6(j)}$	$D_{2(i)\,2(j)\,8(k)}$ $D_{2(i)\,4(j)\,6(k)}$ $D_{4(i)\,4(j)\,4(k)}$	7	4
16	$D_{16(i)}$	$D_{2(i)\,4(j)}$ $D_{4(i)\,12(j)}$ $D_{6(i)\,10(j)}$ $D_{8(i)\,8(j)}$	$D_{2(i)\,2(j)\,12(k)}$ $D_{2(i)\,4(j)\,10(k)}$ $D_{2(i)\,6(j)\,8(k)}$ $D_{4(i)\,4(j)\,8(k)}$ $D_{4(i)\,6(j)\,6(k)}$	10	5
18	$D_{18(i)}$	$D_{2(i)\,16(j)}$ $D_{4(i)\,14(j)}$ $D_{6(i)\,12(j)}$ $D_{8(i)\,10(j)}$	$D_{2(i)\,2(j)\,14(k)}$ $D_{2(i)\,4(j)\,12(k)}$ $D_{2(i)\,6(j)\,10(k)}$ $D_{2(i)\,8(j)\,8(k)}$ $D_{4(i)\,4(j)\,10(k)}$ $D_{4(i)\,6(j)\,8(k)}$ $D_{6(i)\,6(j)\,6(k)}$	12	7

ble the corresponding experimental out-of-roundness profiles;

(b) verifying the adequacy of the derived slowness surface particularly by a systematic comparison of experimental out-of-roundness profiles with predicted

profiles. This step, which needs attention, will be reported in a future paper. Let us only remark that in the present work the verification step includes both analyses related to the etching of cylindrical crystals and to the etching of rough surfaces.

We apply this procedure to the anisotropic etching of KOH on silicon crystal to evaluate 24 dissolution constants related to tensors of ranks 12–18.

After some adjustments we have generated [52] the dissolution slowness surface shown in Fig. 16d–f. The observation direction, D_{obs}, which lies normal to the plane of the figure, is respectively taken along the [0 1 0], [1 1 0] and [1 1 1] axes. Hence, one may verify that the derived slowness surface satisfies the crystal symmetry. At first sight the slowness surface seems to be composed of eight elongated lobes aligned along $\langle 1 1 1 \rangle$ axes. However, the slowness surface exhibits several other less-accentuated peaks, such as maxima lying along $\langle 1 0 0 \rangle$ axes.

At this point one may remark that is should be more appropriate to present polar diagrams of L in the form L ($\varphi = \varphi_0$, θ) to appreciate the variations in L with the angles of cut. Such polar diagrams will be extensively reported in Part II of this work with, in addition, the theoretical two-dimensional etched shapes, such as out-of-roundness profiles as numerically derived from these diagrams. However, to illustrate the adjustment of the dissolution constants which generate the (0 1 0) polar diagram for L we have drawn in Fig. 1 (dashed curve) the theoretical curve which describes the variations in Δd ($\Delta d/t = 2R$ with $R = [L(\varphi_0, \theta_0 = 0°)]^{-1}$) with the angle of cut φ_0. Small discrepancies (typically less than 5%) between the experimental and theoretical curves are obtained as φ_0 increases from 0° to 45°.

5. Conclusion

The 35% KOH solution is found to etch anisotropically differently oriented crystalline silicon plates. Prolonged etching causes the development of dissolution shapes characteristic of the angles of cut. In particular, all the out-of-roundness profiles are found to reflect the crystal symmetry. The surface texture which results from repeated etchings is connected with the presence of extrema in the dissolution slowness in the vicinity of the reference surface.

The tensorial representation of the anisotropic dissolution process is then fully appropriate to describe the observed orientation effects. Conditions to derive the dissolution slowness surface for crystalline silicon are then met in this experimental study. After a complete analysis of data it has been possible to estimate the dissolution constants involved in the equation expressing L (φ, θ). The only condition for obtaining a slowness surface with a shape sufficiently complicated to explain the anisotropy is to work with tensors of very high rank (typically $N_{max} > 12$).

It is evident that to appreciate the adequacy of the proposed slowness surface we have to compare systematically various experimental and theoretical dissolution shapes. Then a full exploitation of the dissolution slowness surface requires the development

of numerical and graphical simulations to predict etched shapes related to initially cylindrical crystals and to profilometry traces. This comparison constitutes the matter for a future paper. Under these conditions, the slowness surface derived in Part I will be used in Part II to predict dissolution shapes, to correlate theory to experiments and to discuss the agreement of the dissolution slowness surface. It is obvious that this future discussion will be rigorous only if we deal with many data related to various singly-rotated silicon plates. The large number of diagrams reported in this paper will be used to provide a complete and consistent discussion.

References

1. K. SANGWAL, "Etching of Crystals" (North-Holland, Amsterdam, 1987).
2. B. A. IRVING, in "The Electrochemistry of Semiconductors", edited by P. J. Holmes (Academic Press, London, 1962) pp. 256–89.
3. R. B. HEIMANN, in "Silicon Chemical Etching", edited by J. Grabmaier (Springer, Berlin, 1982) pp. 197–224.
4. M. W. WEGNER and J. M. CHRISTIE, Phys. Chem. Minerals. 9 (1983) 67.
5. C. R. TELLIER, Surf. Technol. 21 (1984) 83.
6. H. C. GATOS and M. C. LAVINE, J. Electrochem. Soc. 107 (1960) 433.
7. M. CASTAGLIOLA, C. R. TELLIER and J. L. VATERKOWSKI, J. Mater. Sci. 21 (1986) 3551.
8. J. W. FAUST, in "The Surface Chemistry of Metals and Semiconductors", edited by H. C. Gatos (Wiley, New York, 1960) p. 151.
9. P. J. HOLMES, in "The electrochemistry of Semiconductors", edited by P. J. Holmes (Academic Press, London, 1962) pp. 329–77.
10. K. E. PETERSEN, Proc. IEEE 70 (1982) 420.
11. G. DELAPIERRE, Sensors and Actuators 17 (1989) 123. ·
12. S. K. CLARK and K. D. WISE, IEEE Trans. Electron Devices ED-26 (1979) 1887.
13. M. BAO and Y. WANG, Sensors and Actuators 12 (1987) 49.
14. K. E. PETERSEN, IEEE Trans. Electron Devices ED-25 (1978) 1241.
15. R. J. WILFINGER, P. H. BARDELL and D. S. CHABRA, IBM J. Res. Devel. 12 (1968) 113.
16. G. KAMINSKY, J. Vac. Sci. Technol. B3 (1985) 1015.
17. A. I. STOLLER, RCA Rev. June (1970) 271.
18. R. A. BUSER and N. F. DE ROOJ, Sensors and Actuators 17 (1989) 145.
19. Y. LINDEN, L. TENERZ, J. TIREN and B. HOK, ibid. 16 (1989) 67.
20. K. YAMADA, M. NISHIHARA, R. KANZAWA and R. KOBAYASHI, ibid. 4 (1983) 63.
21. G. BLASQUEZ, P. PONS and A. BOUKABACHE, ibid. 17 (1989) 387.
22. W. H. KO, J. HYNECEK and S. F. BOETTCHER, IEEE Trans. Electron Devices ED-26 (1979) 1896.
23. H. SEIDEL and L. CSEPREGI, Sensors and Actuators 4 (1983) 455.
24. H. SEIDEL, L. CESEPREGI, A. HEUBERGER and H. BAUMGARTEL, J. Electrochem. Soc. 137 (1990) 3613.
25. D. B. LEE, J. Appl. Phys. 40 (1969) 4569.
26. K. E. BEAN, IEEE Trans. Electron Devices ED-25 (1978) 1185.
27. M. J. DECLERCQ, L. GERZBERG and J. M. MEINDI, J. Electrochem. Soc. 122 (1975) 545.
28. M. M. ABU-ZEID, ibid. 134 (1984) 2138.
29. X. P. WU and W. H. KO, Sensors and Actuators 18 (1989) 207.
30. Y. KANDA and A. YASUKAWA, Sensors and Actuators 2 (1982) 283.
31. Y. KANDA, ibid. 4 (1983) 199.
32. Y. WANG, M. BAO and L. YU, ibid. 18 (1989) 221.

33. F. C. FRANK, in "Growth and Perfection of Crystals", edited by R. H. Doremus, B. W. Robert and D. Turnbull (Wiley, New York, 1965) p. 411.
34. F. C. FRANK and M. B. IVES, *J. Appl. Phys.* **31** (1960) 1996.
35. D. W. SHAW, *J. Electrochem. Soc.* **128** (1981) 874.
36. *Idem. J. Crystal Growth* **47** (1979) 509.
37. C. R. TELLIER and J. L. VATERKOWSKI, *J. Mater. Sci.* **24** (1989) 1077.
38. C. R. TELLIER and T. G. LEBLOIS, in "Proceedings of the Third European Time and Frequency Forum, Besançon, France, 1989 (Imprimerie Conseil Général du Doubs, Besançon, 1989) pp. 246–55.
39. C. R. TELLIER, *J. Crystal Growth* **100** (1990) 515.
40. C. R. TELLIER, T. G. LEBLOIS and P. C. MAITRE, *J. Mater. Sci.* **24** (1989) 3029.
41. A. BRAHIM-BOUNAB, J. Y. AMAUDRUT, C. R. TELLIER, *ibid.* **26** (1991) 5585.
42. C. R. TELLIER, J. Y. AMAUDRUT and A. BRAHIM-BOUNAB, *ibid.* **26** (1991) 5595.
43. T. LEBLOIS and C. R. TELLIER, *J. Phys. III* **2** (1992) 1259.
44. A. BRAHIM-BOUNAB and C. R. TELLIER, in "Proceedings of the 6th European Frequency and Times Forum", Noordwijk, The Netherlands, March 1992 (European Space Agency, Paris, 1992) pp. 355–60.
45. C. R. TELLIER, T. LEBLOIS, A. BRAHIM-BOUNAB and D. BENMESSAOUDA, in "Proceedings of the 1st Japanese-French Congress of Mecatronique", Besançon, France, October 1992 (Imprimerie du Conseil Général du Doubs, Besançon, 1992) 6 pp.
46. C. R. TELLIER and F. JOUFFROY, *J. Mater. Sci.* **18** (1983) 3621.
47. C. R. TELLIER, in "Proceedings of the 39th Annual Symposium on Frequency Control", Philadelphia, PA, May 1985 (Institute of Electronic and Electrical Engineers, New York, 1985) p. 282.
48. A. P. HONESS, "The Nature, Origin and Interpretation of the Etch Figures on Crystals" (Wiley, New York, 1927) Chs III and VI.
49. C. R. TELLIER, P. BLIND and D. JOZWICK, in "Proceedings of the 2nd European Frequency and Time Forum", Neuchâtel, Switzerland, March 1988 (Fondation Suisse pour la Recherche en Microtechniques, Neuchâtel, 1988) pp. 937–58.
50. B. A. IRVING, *J. Appl. Phys.* **31** (1960) 109.
51. "Standard on Piézoelectricity" (IEEE, New York, 1978) p. 15.
52. A. BRAHIM-BOUNAB, Thesis 279, University of Franche-Comté, Besançon, France, 25 September 1992.